A fast bipolar H₂ outflow from IRAS 16342-3814: an old star reliving its youth

T.M. Gledhill[1]⋆, K.P. Forde[1]

[1]*Science and Technology Research Institute, University of Hertfordshire, College Lane, Hatfield AL10 9AB, UK*

6 December 2011

ABSTRACT

Some evolved stars in the pre-planetary nebula phase produce highly-collimated molecular outflows that resemble the accretion-driven jets and outflows from pre-main sequence stars. We show that IRAS 16342-3814 (the Water Fountain Nebula) is such an object and present K-band integral field spectroscopy revealing a fast (> 150 km s^{-1}) bipolar H₂ outflow. The H₂ emission is shock excited and may arise in fast-moving clumps, accelerated by the previously observed precessing jet. The total luminosity in H₂ is 0.37 L$_\odot$ which is comparable with that of accretion-powered outflows from Class 0 protostars. We also detect CO overtone bandhead emission in the scattered continuum, indicating hot molecular gas close to the centre, a feature also observed in a number of protostars with active jets. It seems likely that the jet and outflow in IRAS 16342-3814 are powered by accretion onto a binary companion.

Key words: circumstellar matter – stars: AGB and post-AGB – stars: evolution – stars: individual: IRAS 16342-3814 – stars: individual: The Water Fountain Nebula – shock waves

1   INTRODUCTION

Imaging studies of pre-planetary nebulae (pre-PN) at optical and infrared wavelengths have revealed a wide range of bipolar, multipolar and point-symmetric structures in scattered and thermal emission from dust (e.g. Lagadec et al. 2011; Siódmiak et al. 2008, Sahai et al. 2007; Gledhill 2005). These nebulae are often accompanied by collimated outflows traced by the rotational lines of CO and other molecules, and the near-infrared ro-vibrational lines of H₂ (e.g. Sahai et al. 2006; Sánchez Contreras et al. 2004; Cox et al. 2003). The process by which the outflows are shaped appears to involve, at least in the case of the more extreme outflows, the appearance of axial jets, which carve out cavities in the circumstellar material (Sahai & Trauger 1998).

This final flourish of activity by low- and intermediate-mass stars at the end of the AGB is remarkably similar to the pre-main sequence (pre-MS) outflow phase of their youth. Disc winds and jets are thought to be an integral part of the star formation process and are seen from the early Class 0 accretion phase through to Class III and final contraction onto the main sequence (e.g. Cabrit, Ferreira & Dougados et al. 2011). Pre-MS jets and outflows often manifest themselves as shock-excited structures such as Herbig-Haro (HH) objects, visible in CO and H₂ emission lines. Although the

mechanism for ejecting and driving pre-MS outflows is still a subject of debate, models fall broadly into the categories of disc winds (Königl & Pudritz 2000) and X-winds (Shu et al. 2000), both of which involve magnetocentrifugal outflows from accretion discs. In the case of pre-PN with bipolar outflows, it has been known for some time that the momentum present in the outflow often greatly exceeds that which could be supplied by a radiation-driven stellar wind (Bujarrabal et al. 2001) so that an additional driving mechanism is required. It seems likely that the additional energy may derive from the presence of a binary companion, either stellar or substellar (review by De Marco 2009), and that accretion may also play a central role in powering these pre-PN outflows.

IRAS 16342-3814 (hereafter IRAS 16342), is one of the "Water Fountain" sources which exhibit high-speed H₂O maser emission. The masers in IRAS 16342 are thought to trace bow shocks at the ends of a jet, with material in the head of the jet travelling at 155 km s^{-1} (Claussen, Sahai & Morris 2009). Infrared imaging shows a spectacular corkscrew feature which has been interpreted as evidence of a precessing jet, actively carving cavities in the dusty molecular envelope (Sahai et al. 2005). In this paper we present integral field spectroscopy in the K-band, using the SINFONI instrument on the VLT, revealing a high-speed bipolar outflow in H₂. We draw comparisions with the well-studied pre-

⋆ email: t.gledhill@herts.ac.uk

PN system CRL 618 and then with pre-MS outflow sources which show strong evidence for accretion-driven jets.

2   OBSERVATIONS AND DATA REDUCTION

Observations of IRAS 16342 were made on 2005 June 29 with the SINFONI integral field spectrometer on the 8.2-m UT4 telescope at the VLT observatory in Chile (Eisenhauer et al. 2003, Bonnet et al. 2004). The K-band grating was used covering a wavelength range of 1.95 to 2.45 µm with spectral resolution of $\sim$ 5000. This equates to a spectral pixel (channel) width of 2.45×10^{-4} µm. The expected full width at half maximum (FWHM) in the spectral direction is 2 channels or 4.9×10^{-4} µm (≈ 66 km s^{-1} at 2.2 µm).

Medium Resolution Mode (MRM) was used providing a field of view of 3×3 arcsec with 50×100 mas spatial pixels. The total integration time on-source was 16 minutes. Offset sky exposures were obtained along with the standard arc, flux and telluric calibrations. Flux and telluric calibration were performed using HD 156152. The average airmass was 1.23 with an ambient seeing of ≈ 0.8 arcsec. Adaptive optics (AO) correction in MRM resulted in a slightly E-W elongated point spread function (PSF) of 0.13×0.10 arcsec FWHM as measured using the standard.

Data reduction was accomplished using the ESO pipeline for SINFONI with further processing and data visualization using the STARLINK software collection. For further details on our processing of the SINFONI data cubes, see Gledhill et al. (2011).

3   RESULTS AND ANALYSIS

The pipeline-reduced and telluric-corrected datacube can be summed over the 1.95 to 2.45 µm wavelength range of SINFONI to form a "white light" image, and this is shown in Fig. 1. The inner structure of the lobes is shown as a greyscale upon which we superimpose contours to illustrate the fainter bipolar nebulosity. The source is hidden behind the central region of obscuration which separates the two lobes and we mark an approximate position as '+', estimated as midway between the pinched isophotes in Fig. 1. In fact the source remains obscured even in mid-infrared observations with $\tau \geqslant 100$ up to 30 μm (Verhoelst et al. 2009; Lagadec et al. 2011). In the K-band the bipolar lobes are seen primarily by dust-scattered light, as indicated by their high degree of linear polarization in this waveband (Murakawa & Sahai 2010).

Our image bears strong similarity to the K_p (1.948 − 2.299 µm) Keck image presented by Sahai et al. (2005) in which they identify structure, including a number of knots, which they attribute to the action of a precessing jet. We indicate in Fig. 1 two knots in each lobe which are common between our image and the K_p image of Sahai et al. (2005), using their nomenclature. The integrated flux in the NE and SW lobes in our data is 32.3 ± 1.5 and 75.2 ± 1.5 mJy respectively, which compares well with the fluxes of 35 and 86 mJy measured by Sahai et al. (2005) through their K_p filter. Our lower flux for the SW lobe is easily explained by the fact that this lobe extends beyond the edge of the
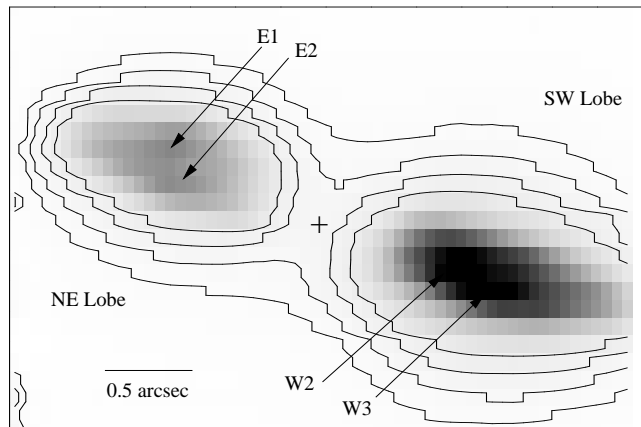

Figure 1. A 'white light' image of IRAS 16342 covering the wavelength range of $1.95 - 2.45$ µm and showing the inner structure in the lobes with contours of the fainter surrounding nebulosity. The locations of the knots identified by Sahai et al. (2005) are indicated. Coutours are at 1.0, 1.6, 2.5, 4.0 with the peak of the greyscale at 55, in units of 10^{-15} W m^{-2} arcsec^{-2}. N is up and E to the left.

SINFONI field of view and so is truncated in our observation (Fig. 1).

3.1 K-band spectrum

In Fig. 2 we show the spectrum of IRAS 16342 between 1.95 and 2.45 µm, showing detection of a number of H$_2$ ro-vibrational lines, with fluxes listed in Table 1. A previous search for H$_2$ emission in 1993 by García-Hernández et al. (2002) resulted in a non-detection with a 2σ upper limit of 5.1×10^{-17} W m^{-2}. It seems likely that their wide slit (4.5 arcsec) oriented at $-70°$ admitted too much continuum to detect the H$_2$ lines, although we cannot rule out the possibility that the H$_2$ emission has brightened between 1993 and 2005. The continuum brightness in the SW lobe is approximately 2.5 times that in the NE lobe, so we show the two spectra separately. Features present in the scattered continuum are more evident in the SW lobe whereas the H$_2$ emission lines are more evident in the NE lobe. In summary we note that: (i) the continuum rises steadily with wavelength, indicating a very red source; (ii) the 1-0 S- and Q-branch ro-vibrational transitions of H$_2$ are strong and we also detect a number of 2-1 transitions. Upon closer inspection, the H$_2$ lines are each doppler split into two components, corresponding to blue-shifted (relative to the systemic velocity) emission in the SW lobe and red-shifted emission in the NE lobe. This is discussed further in Section 3.4; (iii) a number of CO first overtone bandheads are seen in emission longward of 2.29 µm; (iv) there is a Na I doublet feature in emission at 2.22 µm.

3.2   H$_2$ line ratios

The $1 - 0$ S(1)/$2 - 1$ S(1) flux ratio is an important excitation diagnostic and has values of ~ 10 and above for shock-excited H$_2$ (e.g. Shull & Hollenbach 1978). As the $2 - 1$ S(1) line is weak in IRAS 16342 (the flux in this line is the same within errors in the two lobes) we calculate a combined ratio

Table 1. Peak wavelength (λ_p), corresponding LSR velocity (V_{LSR}) and line flux (F) for the continuum-subtracted H$_2$ lines, shown separately for the NE and SW lobes. Flux units are 10^{-18} W m^{-2}, wavelengths in microns and velocities in km s^{-1}. The uncertainty on the velocity is estimated at 0.5 spectral channels, or 17 km s^{-1}. The rest wavelength for each line (λ_0) is also given (Bragg, Brault & Smith 1982).

| Line	λ_0	NE lobe			SW lobe		
		λ_p	V_{LSR}	F	λ_p	V_{LSR}	F
1-0 S(3)	1.9576	1.9585	+139	15.6 ±1.0	1.9571	-87	18.6 ±1.2
1-0 S(2)	2.0338	2.0350	+174	6.60 ±0.81	2.0330	-115	9.37 ±1.13
2-1 S(3)	2.0735	2.0747	+164	1.71 ±0.74	2.0730	-84	2.52 ±1.06
1-0 S(1)	2.1218	2.1229	+150	26.1 ±0.9	2.1212	-88	40.0 ±1.5
1-0 S(0)	2.2235	2.2246	+144	6.24 ±0.76	2.2229	-87	9.95 ±1.31
2-1 S(1)	2.2477	2.2491	+183	2.15 ±1.06	2.2469	-112	2.69 ±1.89
1-0 Q(1)	2.4066	2.4079	+153	28.8 ±0.9	2.4059	-91	43.0 ±1.3
1-0 Q(2)	2.4134	2.4147	+160	9.21 ±0.91	2.4128	-84	11.7 ±1.1
1-0 Q(3)	2.4237	2.4250	+158	27.3 ±1.1	2.4231	-85	39.7 ±1.8
1-0 Q(4)	2.4375	2.4387	+147	6.30 ±0.97	2.4368	-94	5.08 ±1.35
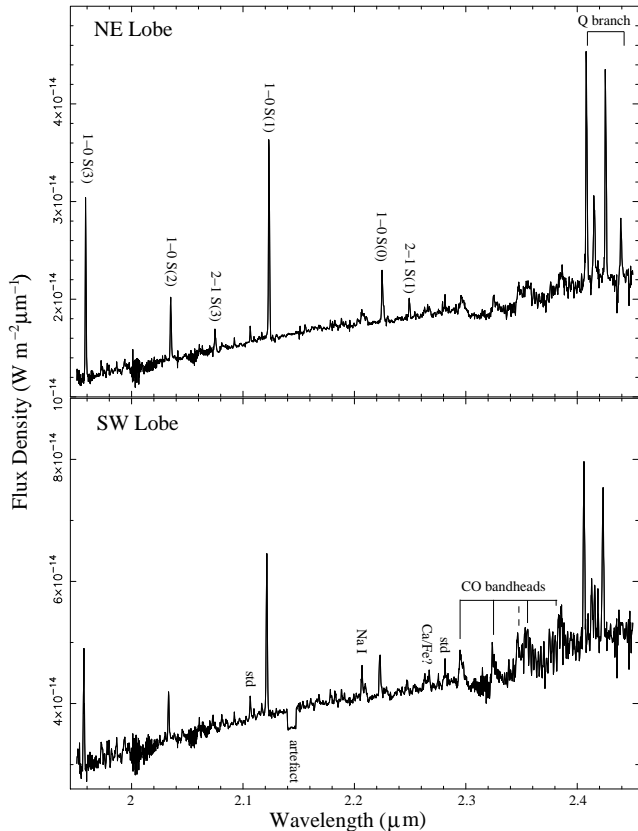
Figure 2. SINFONI spectra of IRAS 16342 integrated over the region of nebulosity bounded by the third contour in Fig. 1. The continuum brightness differs by a factor of $\approx$ 2.5 between the two lobes and so we show them separately. The H$_2$ emission lines are labelled in the top diagram and other features in the lower diagram. The ^{13}CO $2-0$ bandhead is indicated with a dotted line. Features due to the telluric standard are shown as "std".

for both lobes, giving $1-0$ S(1)/$2-1$ S(1)=13.7±6.1, which is indicative of shock-excited H$_2$.

Any line of sight extinction will cause this ratio to increase, remaining consistent with a shock interpretation. An estimate of the line of sight extinction from the H$_2$ emitting region to the observer can be obtained from the ratio of the $1-0$ Q(3) and $1-0$ S(1) lines and the assumption of a power law dependence of extinction with wavelength across the K-band (e.g. Davis et al. 2003). A value of -1.75 has often been assumed for the power law exponent of the near-infrared extinction law, however we assume that $A_\lambda \propto \lambda^{-2.14}$ for the K-band, which has been estimated for the Galactic plane (Stead & Hoare 2009) and is also consistent with lines of sight towards the Galactic Centre (Schödel et al. 2010). Using the $1-0$ Q(3) and $1-0$ S(1) line strengths in Table 1 gives an extinction at the wavelength of the $1-0$ S(1) line of $A_{1-0\ \text{S}(1)} = 1.77 \pm 0.23$ and 1.54 ± 0.26 magnitudes for the NE and SW lobes respectively. Although a higher extinction towards the NE lobe would be consistent with the tilt of the bipolar axis determined from previous studies (e.g. Claussen et al. 2009) the two lobes have the same extinction within our error. Using the combined fluxes for both lobes gives an extinction of $A_{1-0\ \text{S}(1)} = 1.63 \pm 0.18$ and an extinction-corrected line ratio of $1-0$ S(1)/$2-1$ S(1)=16.3 ± 9.1.

A shock-excitation interpretation is also supported by the non-detection of higher vibrational transitions, such as the $3-2$ S(3) line at 2.2014 µm.

3.3 H$_2$ Excitation

In Fig. 3 we plot a ro-vibrational diagram showing column densities of H$_2$ for the lines in Table 1, relative to the $1-0$ S(1) line. For a single temperature LTE gas the points will lie along a straight line. We plot points for the NE and SW lobes separately, each corrected with the extinction estimates derived in the previous section. With the exception of the $1-0$ Q(4) line in the SW lobe (at $T_{\text{upper}} = 7586$ K), the Q-branch and S-branch transitions deriving from the same upper energy level agree well indicating that the correction for differential extinction is good. The $1-0$ Q(4) flux appears anomalous (being the only line in which the SW lobe is fainter than the NE lobe) and suffers from a noisy continuum subtraction, lying at the long-wavelength limit of the instrument. A weighted least-squares fit to the $v = 1-0$ transitions, excluding this point, gives a gas temperature of 1394 ± 51 K. Although the $v = 2-1$ transitions could be fitted within error by a line of similar slope, they are clearly
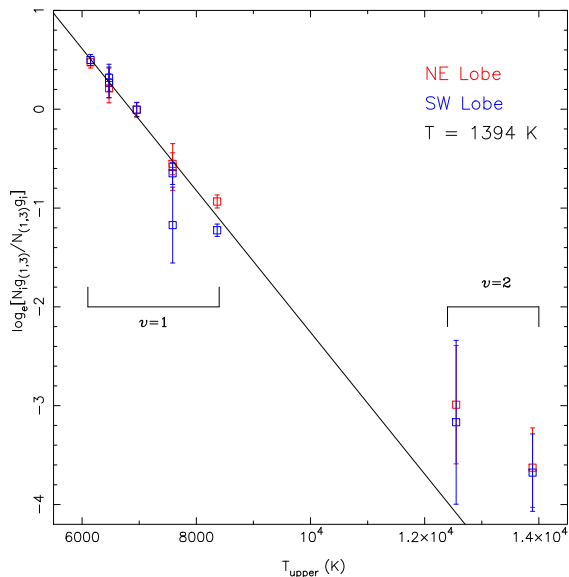
Figure 3. An excitation diagram showing the log of the normalized column densities against upper level temperature for the lines in Table 1. Red and blue symbols represent the NE and SW lobes respectively. A weighted least-squares fit to the $v = 1 - 0$ transitions (excluding the $1 - 0$ Q(4) SW lobe point) corresponds to a LTE gas temperature of 1394 K.

offset from the $v = 1 - 0$ fit so that the vibrational temperature is hotter by $400 - 600$ K (for S(3) and S(1) lines respectively). An offset between the vibrational levels can result in regions where the shocked gas is not fully thermalised and this is seen in 3D models of bow shocks (e.g. Gustafsson et al. 2010). There is also evidence for a similar offset in the H_2 ro-vibrational diagram for CRL 618, a pre-PN also with a fast H_2 outflow (Thronson 1981) and discussed further in Sec. 4.2.

3.4 H_2 spatial distribution

The relative locations of the H_2 emission and the scattered continuum are shown in Figs. 4 and 5 for the $1 - 0$ S(1) line (other lines show a similar structure). In the accompanying spectrum to Fig. 5 the line is clearly split into blue- and red-shifted components, relative to a central wavelength of 2.1222 μm. A similar split is seen in the other H_2 lines. The blue-shifted emission is associated with the SW lobe and the red-shifted emission with the NE lobe (a small amount of blue (red) emission appears in the NW (SE) lobe close to the central wavelength due to the spectral PSF of SIN-FONI). The peak of the H_2 emission in each lobe is located at a greater angular offset from the centre than the knots, which are thought to represent enhanced scattering from denser material swept up in the lobe walls. The peaks occur close to the axis of the system at PA 68°, defined by the scattered light image, but their offset along this axis is not symmetrical with respect to the centre of the obscuring lane (marked '+'); the NE (red shifted) H_2 peak lies at an offset of 1.0 arcsec whereas the SW (blue shifted) peak forms an elongated feature lying between 1.3 and 1.5 arcsec offset. However the continnum contours show that the lobes
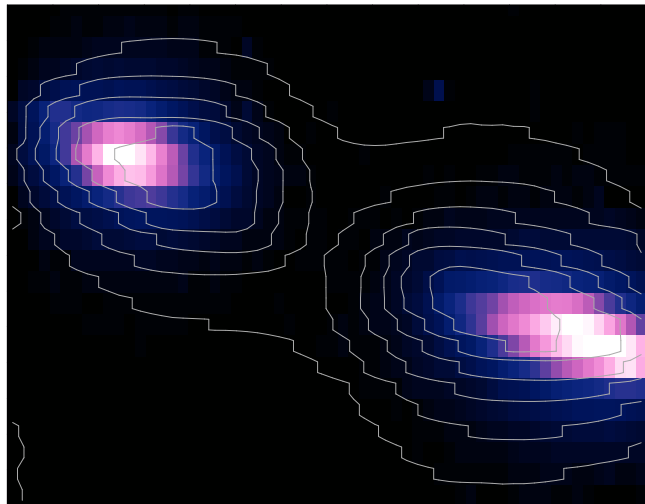

Figure 4. An image of the $1 - 0$ S(1) line emission with K-band white light contours (from Fig. 1), showing the relative locations of the H_2 and the scattered continuum. The peak of the colour scale (white) corresponds to 1.9×10^{-16} W m^{-2} arcsec^{-2}.

are not of equal size, with the larger SW lobe extending beyond our field of view. Relative to the outer continuum contour, the H_2 peaks do seem to occupy a symmetrical position, being set back by approximately 0.56 arcsec from the tips of both lobes (estimated in the case of the SW lobe). It is notable from the contours in Fig. 5 that the peak H_2 surface brightness is very similar in both lobes, despite the continuum brightness being a factor 2.5 higher in the SW lobe (contours in Fig. 4).

The locations of the V_{LSR}=+153, +178.7 and -66 km s^{-1} H_2O maser clumps detected in 2002 VLBA observations (Claussen et al. 2009) are shown in Fig. 5. Using the proper motions established by these multi-epoch measurements, we have adjusted the maser positions to account for the 3 year interval between the VLBA and SINFONI observations. We set the origin in our data as the centre of the obscuring lane and plot the maser positions relative to this point (marked '+' in Fig. 5). All three H_2O maser clumps are located close to the axis of the nebula, as indicated by the dotted line, but are slightly offset to the N (S) in the NE (SW) lobes in a point-symmetric fashion, and lie along an axis at PA 66°. These offsets are interpreted by Claussen et al. (2009) as further evidence for the presence of a precessing jet.

3.5 H_2 kinematics

The spectral separation between the two $1-0$ S(1) line peaks (7 SINFONI channels, or 1.715×10^{-3} μm) corresponds to a velocity separation of 238 km s^{-1}. The LSR velocities of the line peaks are -88 and $+150$ km s^{-1} with a central velocity (midway between the two peaks) of $+31$ km s^{-1}. A cautious error estimate of half a spectral pixel corresponds to ± 17 km s^{-1}. Velocities of the various line peaks are given in Table 1.

A systemic velocity for IRAS 16342 of 43.2 ± 0.9 km s^{-1} was determined by Likkel, Morris & Maddalena (1992), by searching for velocity-symmetric H_2O maser pairs, in agree-
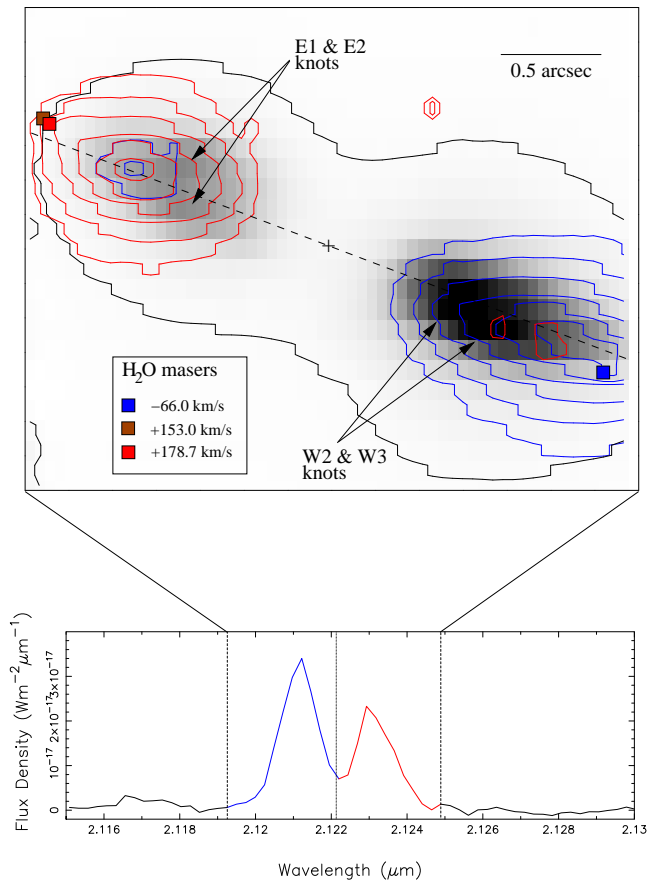
Figure 5. Contours of 1-0 S(1) H_2 emission, extracted and colour coded according to the spectrum in the lower panel, superimposed on the greyscale white-light image from Fig. 1. The outer contour from Fig. 1 is included to show the faint scattered light structure, with the symmetry axis shown as a dotted line at PA 68°. The centre of the K-band obscuration is marked '+'. The systemic velocity of 42 km s^{-1} derived from maser observations is shown as a dotted line on the spectrum. H_2 contour levels are 2, 4, 8, 16, 32, 63 ×10^{-17}W m^{-2} arcsec^{-2}. The locations of the VLBA H_2O masers from Claussen et al. (2009) are shown.

ment with Likkel & Morris (1988) and te Lintel Hekkert et al. (1988). Sahai et al. (1999) estimate 42 ± 2 km s^{-1} from the OH masers, and the more recent H_2O maser study by Claussen et al. (2009) assumes this value. Taking the systemic velocity and outflow axis inclination as $+42\pm2$ km s^{-1} and 45° from the maser observations, then the H_2 outflow velocity relative to the source (i.e. along the bipolar axis) is 153 and 184 ± 24 km s^{-1} in the NE and SW lobes repectively. A higher outflow velocity in the SW lobe may be consistent with the H_2-emitting region in that lobe being located further ($1.3 - 1.5$ arcsec) from the source than in the NE lobe (1.0 arcsec), although within our errors the outflow velocities in the two lobes could be the same.

The $+153$ km s^{-1} maser clump at the tip of the NE lobe shares a very similar velocity with the red-shifted peaks of the bright $1-0$ S(1), Q(1) and Q(3) H_2 lines ($V_{LSR} = +150$, $+153$ and $+158$ km s^{-1} respectively). The other red-shifted H_2 lines also have velocities consistent with $+153$ km s^{-1} to within ±17 km s^{-1} (±0.5 spectral channel), apart from the $2-1$ S(1) line, which has a peak at $+183$ km s^{-1}, and

the $1 - 0$ S(2) line at $+174$ km s^{-1}. The latter two lines are more comparable with the $+178.7$ km s^{-1} maser (see Table 1). These velocity associations in the NE lobe suggest that the H_2O maser and H_2 emission may originate within gas sharing similar bulk motion. In the SW lobe, the bright $1 - 0$ S(1), Q(1) and Q(3) lines peaks are blue-shifted at $V_{LSR} = -88$, -91 and -85 km s^{-1} respectively. Although we have not imaged the tip of this lobe, we appear to have imaged the peak of the H_2 emission, which lies close to the blue-shifted maser clump at -66 km s^{-1}, again suggesting similar bulk motion in the gas responsible for the H_2 and H_2O emission. As in the NE lobe, the $1-0$ S(2) and $2-1$ S(1) lines show higher velocities.

3.5.1 Line profiles

To investigate the H_2 kinematics further we plot a position-velocity (P-V) diagram obtained by simulating an 8-pixel (0.4 arcsec) wide slit oriented along the major axis of the nebula (the dashed line in Fig. 5). This is shown in Fig. 6 (centre) along with a number of velocity slices taken at various offsets along the 'slit' (top and bottom). We note the following features:

(i) The slices show that the peak flux density in the $1 - 0$ S(1) line is approximately the same in both lobes (panels b and e) despite the continuum peak in the SW lobe being a factor 2.5 times brighter than in the NE lobe. This suggests that the temperature and column density of shocked H_2 are similar in both lobes and that the higher continuum flux in the SW lobe is due to a forward-scattering dust phase function rather than an increase in dust and gas density.

(ii) The line broadens as we move from the tips of the lobes towards the source (from $a \rightarrow c$ and from $f \rightarrow d$). The line profiles in Fig. 6 indicate a wide range of velocities, with FWHM ~ 200 km s^{-1}.

(iii) The line becomes increasingly asymmetric moving from the lobe tips towards the source, so that in the NE (red shifted) lobe it develops a red wing (panels $a \rightarrow c$) whereas in the SW (blue shifted) lobe a blue wing develops (panels $f \rightarrow d$), eventually splitting into two velocity components in the P-V diagram.

(iv) We do not see any clear evidence for a shift in the line peak (increase in outflow velocity) with offset from the star.

Schultz et al. (2005) present a gallery of H_2 line profiles for bow shocks with a range of geometries, inclinations and shock velocities. These show line widths $\sim V_{bow}$, where V_{bow} is the velocity of the bow relative to the ambient medium, so that fast bow shocks are expected to produce broad H_2 emission lines. In the case of an inclined outflow axis (45° for IRAS 16342, Claussen et al. 2009), then the line profile can become asymmetric with a high-velocity wing arising from the bow apex and the core of the line resulting from the larger area of lower-velocity gas in the near surface of the shock. Although asymmetric line profiles are evident in our data (Fig. 6), the high velocity wings become stronger at positions c and d, *further* from the bow apex and closer to the source, which is hard to interpret as a simple terminal bow shock. This is discussed further in Sec. 4.3.
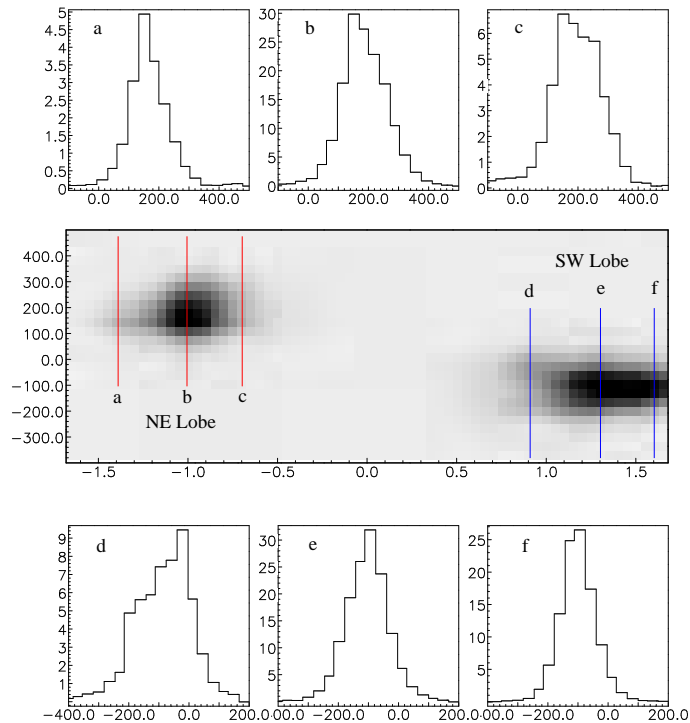
Figure 6. The central panel shows a P-V diagram with arcsec offset along the the horizontal axis and V_{LSR} in km s^{-1} along the vertical axis. Slices of H$_2$ surface brightness in the velocity direction (km s^{-1}) are shown at six positions along the outflow axis. The H$_2$ surface brightness is in units of 2×10^{-19} W m^{-2} μm^{-1} arcsec^{-2}.

3.6   Mass of the H$_2$ outflow

The flux in the $1 - 0$ S(1) line can be used to estimate the mass of shocked H$_2$ in the outflow, following the procedure outlined by Davis et al. (2001). For a gas excitation temperature of 1400 K (Sec. 3.2), the column density of H$_2$ in m^{-2} is given by $N_{\mathrm{H}_2} = 7.596 \times 10^{28} I_{1-0S(1)} 4/(a\pi)$, where $I_{1-0S(1)}$ is the extinction-corrected flux in the $1 - 0$ S(1) line in W m^{-2} and a is the solid angle subtended by the H$_2$-emitting region at the observer. Multiplying by the area of the H$_2$ emitting region (in m^2) and the mass of the H$_2$ molecule then gives the mass of shock-excited H$_2$, which can be expressed as $M_{\mathrm{H}_2} = 1.620 \times 10^5 I_{1-0S(1)} d^2$ M$_\odot$ where d is the distance to the object in pc. Taking the flux in both lobes (Table 1) and correcting for an extinction at 2.122 μm of 1.63 ± 0.3 mag. (Sec. 3.1) gives $I_{1-0S(1)} = 2.97 \pm 0.83 \times 10^{-16}$ W m^{-2}. The distance estimate for IRAS 16342 ranges from 700 pc (Zijlstra et al. 2001) to 2 kpc (Sahai et al. 1999). The latter was assumed by Claussen et al. (2009) to determine the tangential H$_2$O maser velocities from their proper motions, which led to an estimate of 45° for the outflow axis, in agreement with independently-derived values. A distance of 700 pc would lead to a much higher inclination (70°). The total mass in H$_2$ is then $M_{\mathrm{H}_2} = 1.92 \pm 0.54 \times 10^{-4} (d/2\mathrm{kpc})^2$ M$_\odot$, with the relatively large error arising from the uncertainty on the extinction and distance estimates. The linear extent of the H$_2$-emitting lobes is ≈ 1.3 arcsec which, correcting for the inclination of 45°, will be traversed in ≈ 112 years by an outflow travelling at 155 km s^{-1}, giving a mass flux of $\dot{M}_{\mathrm{H}_2} = 1.7 \pm 0.7 \times 10^{-6} (d/2\mathrm{kpc})$ M$_\odot$ yr^{-1} in H$_2$, assuming

an uncertainty of 20 km s^{-1} on the outflow velocity. For a gas with temperature $T = 2000$ K then M_{H_2} and $\dot{M}_{\mathrm{H}_2}$ are a factor ~ 3 lower.

3.7   CO bandhead and Na I emission

We detect the $v = 2-0, 3-1, 4-2$, and $5-3$ ^{12}CO overtone bandheads in emission. We also see the $v = 2-0$ ^{13}CO bandhead, again in emission as indicated in Fig. 2. The presence of the ^{13}CO bandhead is consistent with the low ^{12}CO/^{13}CO line ratio from millimetre data obtained by He et al. (2008) and interpreted as possible evidence for hot-bottom burning and hence a high-mass progenitor for IRAS 16342. We estimate that the flux in the $v = 2-0$ and $3-1$ ^{12}CO features is 1.4 ± 0.3 and $2.6 \pm 0.5 \times 10^{-17}$ W m^{-2} with large uncertainties due to the difficulty in subtracting a continuum in this region.

A Na I doublet feature is seen in emission with peaks at 2.2069 and 2.2098 μm. The integrated flux across the feature is $1.24 \pm 0.16 \times 10^{-17}$ W m^{-2}.

Our integral field observations show that these spectral features have the same spatial distribution as the continuum and hence originate from a compact source in the central region, obscured from direct view, and are scattered into our line of sight by dust in the bipolar lobes. This is in contrast to the H$_2$ emission which traces the extended bipolar outflow. The situation is remarkably similar to that of IRAS 18276-1431 discussed by Gledhill et al. (2011), where the CO and Na I emission was interpreted as evidence for the presence of hot (> 2000 K) and dense ($> 10^{10}$ cm^{-3}) gas close to the central star(s).

4   DISCUSSION

4.1   CO rotational emission in IRAS 16342

CO emission has been detected toward IRAS 16342 in both the $J = 2-1$ and $J = 3-2$ lines (He et al. 2008; Imai et al. 2009). Although spatially-resolved observations are not yet available, association with interferometric maser data on the basis of velocity gives an indication of the likely CO structure. He et al. (2009) associate the $J = 2-1$ emission (expansion velocity 46 km s^{-1}) with the OH main-line masers which trace the base of the optical/infrared bipolar lobes (Sahai et al. 1999). The larger CO $J = 3-2$ velocity extent of 158 km s^{-1} (Imai et al. 2009) is more comparable with that of the OH 1612 MHz masers (130 km s^{-1}; Sahai et al. 1999; Zijlstra et al. 2001) which are located further from the star, along the edges of the NE and SW lobe. This then gives the picture of CO gas accelerating with offset from the star.

Imai et al. (2009) derive a mass-loss rate of $\dot{M}_{\mathrm{gas}} = 2.9 \times 10^{-5}$ M$_\odot$ yr^{-1} from the CO $J = 3-2$ line. This compares with 1.7×10^{-5} M$_\odot$ yr^{-1} obtained by He et al. (2008)[1] from CO $J = 2-1$ measurements. Both values are greater, by at least a factor of 10, than our estimate from the H$_2$ emission. However, as noted by Imai et al. (2009) the CO mass-loss rates are almost certainly over-estimated due to the assumption of spherical symmetry. Conversely,

---

[1] after a correction applied by Imai et al. (2009)

it is likely that our value of $\dot{M}_{H_2} = 1.7 \times 10^{-5} M_\odot \ \mathrm{yr}^{-1}$ (Sec. 3.4) will be an underestimate since it only accounts for the component of cooling H_2 that has been shock heated by the jet.

Imai et al. (2009) devlop a spatio-kinematic (SHAPE) model to fit the CO $J = 3 - 2$ line profile and conclude that, while their model is not unique, the emission is consistent with a bipolar CO flow with outflow velocity proportional to distance from the star and an exponentially decreasing gas density. The CO and OH emission then traces material that is being accelerated and swept-up into the bipolar cavity walls by the high-speed axial jet, transferring momentum as it goes.

In contrast, the H_2 emission shows no evidence for a low-velocity component and instead appears to be associated purely with the high velocity axial jet, with velocities in both lobes comparable to the H_2O masers at the jet tips. Also, there is no clear evidence in H_2 for the velocity-offset relation seen in the CO and OH data, which is again consistent with the H_2 emission arising in an axial jet rather than in accelerating swept-up cavity wall material.

4.2 Comparison with CRL 618

4.2.1 H_2 emission

The spatial and kinematic structure of the H_2 emission in IRAS 16342 bears a number of resemblances to that of the bipolar proto-PN CRL 618, which also displays shock excited H_2 (Thronson 1981)[2]. Firstly, Cox et al. (2003) map the $1 - 0$ S(1) line in CRL 618 with 0.5 arcsec and 9 km s^{-1} resolution and find that the velocity-integrated emission has a lobe-filled structure, as seen in IRAS 16342, with the emission peaks located close to the nebula axis, rather than along the edges of the lobes. Secondly, high velocity wings in the $1 - 0$ S(1) line were noted in CRL 618 by Burton & Geballe (1986) with a line width of ≈ 250 km s^{-1} (c.f. ≈ 240 km s^{-1} line peak separation in IRAS 16342; Sec 3.2.1), indicating a high-velocity outflow. Spectral imaging with a velocity resolution of 4 km s^{-1} (Kastner et al. 2001) shows that H_2 emission up to 120 km s^{-1} (line of sight) is present in both lobes. This is confirmed by Cox et al. (2003) who show that the high-velocity H_2 is associated with jets traced in optical data, with emission peaking behind the jet heads and extending downstream towards the star. Velocities of 140 km s^{-1} (relative to systemic) behind the jet head in the E lobe correspond to an outflow velocity of 260 km s^{-1} assuming an inclination of $32°$ relative to the plane of the sky (Sánchez Contreras et al. 2004; hereafter SC04). This jet speed is higher than that of IRAS 16342, where the average of the two lobes is 169 km s^{-1} from the H_2 data (Sec. 3.2.1) and 153 km s^{-1} from the H_2O masers (Claussen et al. 2009).

There are also some notable differences between the two objects. The H_2 position-velocity (P-V) diagram for CRL 618 (Cox et al. 2003) shows a characteristic "butterfly" structure, resulting from the presence of both an extended low-velocity component and a high velocity compo-

nent which terminates closer to the star (within ± 2 arcsec along the axis). Although our velocity resolution is much lower, we are confident of the absence of such a butterfly structure in the P-V diagram of IRAS 16342. The line widths do broaden closer to the star, but there is no evidence for a low-velocity component. In CRL 618, low-velocity H_2 emission is associated with the expanding cavity walls and high-velocity emission with the optical jets. In IRAS 16342 the H_2 emission appears to be exclusively associated with the high-velocity axial jet.

4.2.2 CO emission

The characteristic butterfly P-V diagram structure, seen in H_2 emission in CRL 618, is also seen in interferometric observations of CO $J = 2 - 1$ (SC04) and to a lesser extent CO $J = 6 - 5$ (Nakashima et al. 2007). The CO $J = 2 - 1$ maps show two outflow components: a fast axial bipolar outflow, peaking within 2 arcsec of the star, and a more spatially extended lower velocity flow which appears limb brightened and traces the optical lobes. SC04 reproduce the CO $J = 2 - 1$ P-V diagram and spatial distribution with a model consisting of a fast (up to 270 km s^{-1}) cylindrical molecular jet which blows along the axis of more slowly expanding (22 km s^{-1}) bipolar elliptical cavities. The high-velocity component (corresponding to the extended wings of the P-V diagram) is created by the axial jet whereas the lower velocity and more spatially extended emission arises from shocks at the surfaces of the expanding cavities. In the case of IRAS 16342, it is not yet clear whether any of the high-velocity CO emission is associated with the jet.

4.3 Jet models

Lee, Hsu & Sahai (2009), building on earlier models of the optical emission (Lee & Sahai 2003), attempt to model the CO and H_2 emission in CRL 618 using both atomic and molecular winds interacting with a spherically symmetric AGB envelope. They find that (i) it is difficult to produce the observed high-velocity CO and H_2 emission along the axis unless the fast wind is intrinsically molecular and (ii) the wind must be collimated, possibly cylindrical as assumed by SC04 (above), rather than radially expanding as in their model. The presence in IRAS 16342 of both fast axial H_2 emission (this paper), and slower CO emission consistent with expanding cavity walls (Imai et al. 2009), suggests a similar model in which an axial jet sweeps up and accelerates material into the walls of bipolar cavities. Such a model is also consistent with the OH maser data (Zijlstra, Matsuura & Dijkstra 2004). The requirement for collimation raises the possibility that the jet may be magnetized (MHD jet models in pre-PN are discussed by García-Segura, Lopez & Franco 2005 and references therein). Highly-polarized OH maser emission has been detected in the blue-shifted part of the 1612 MHz spectrum (Szymczak & Gérard 2004), implying the presence of magnetic fields in the SW lobe at least.

4.3.1 Precessing jets

The inscribed corkscrew pattern seen in NIR images (Sahai et al. 2005) provides evidence for the presence of a precessing

---

[2] although given the B0 or earlier central star and centrally located HII region in CRL 618 (Westbrook et al. 1975; Schmidt & Cohen 1981) a fluorescent component in this object also seems likely

jet in IRAS 16342, with at least 1.5 rotations visible in the NE lobe (knots E4 to E1) and 3 in the SW lobe (knots W1 to W4). This structure, seen in scattered light, is thought to result from the jet acting as a snow plough, piling up dusty material into a helical density enhancement, as it expands away from the source. Using an average offset between adjacent turns in the corkscrew feature of 0.28 arcsec, $d = 2$ kpc, an outflow speed of 90 km s^{-1} and an inclination of the symmetry axis to the line of sight of $i = 40°$, Sahai et al. (2005) estimate that the precession period is $t_p \leqslant 50$ yr. Taking instead our H$_2$ outflow velocity of 155 km s^{-1} as typical of the jet propagation speed and $i = 45°$ from the H$_2$O maser observations, then $t_p = 24$ yr. This faster precession speed is more compatible with the number of observed turns in the jet and a jet dynamical age of $110 - 130$ yr inferred from the H$_2$O masers (Claussen et al. 2009).

Hydrodynamic models of molecular jets have been produced to simulate observed molecular outflows from protostellar sources (e.g. Suttner et al. 1997; Smith, Suttner & Yorke 1997). Models with both slow ($t_p = 400$ yr) and fast ($t_p = 50$ yr) precessing jets are described by Smith & Rosen (2005) and Rosen & Smith (2004) respectively. These models are able to reproduce some of the basic features of the molecular observations of IRAS 16342 and CRL 618, such as the presence of $1 - 0$ S(1) emission within the body of the outflow surrounded by lower excitation CO $J = 2 - 1$ delineating the outflow lobes. The fast-precessing jet model of Rosen & Smith (2004) seems most closely matched with IRAS 16342, having a jet velocity of 100 km s^{-1}, precession period of $t_p = 50$ yr and precession angles (half angle of the precession cone) of 5, 10 and 20°. Using the locations of the near-infrared knots we estimate the precession angle for IRAS 16342 to be $\approx 10°$ when corrected for the system inclination of 45° to the plane of the sky. The jet diameter is assumed to be 114 au in the models, which is very similar to the $\leqslant 100$ au deduced by Sahai et al. (2005) from the width of the corkscrew pattern. Rosen & Smith present synthetic images of H$_2$ and CO emission which show that the $1 - 0$ S(1) emission develops as an annular structure before breaking into multiple bow shocks. Low excitation CO (e.g. $J = 2 - 1$) traces the walls of the precessional cone with higher excitation lines (e.g. $J = 6 - 5$) contributing to emission from the jet. This is similar to the structure observed in CRL 618 (see fig. 1 of Lee et al. 2009). In the case of IRAS 16342, resolved imaging of the CO lines is needed to determine whether its molecular outflow is similar to that of CRL 618, although the model of Imai et al. 2009 would be consistent with this picture.

In the Rosen & Smith (2004) models, the action of a narrow precessing jet is to excavate an annular region rather than a hollow cavity, leaving a core of relatively undisturbed material along the axis. This is at odds with observations which suggest that the lobes in IRAS 16342 have interiors that are tenuous compared with their walls (Sahai et al. 2005). This may indicate that the cavities in IRAS 16342 were not in fact created by the jet, but predate it.

4.3.2 H$_2$ dissociation and fast-moving clumps

A further problem with the shock models as they stand is that they do not produce the high-velocity H$_2$ emission observed in IRAS 16342, CRL 618 and many YSO outflows,

due to the dissociation of H$_2$ molecules at hydrodynamic shock speeds of $\leqslant 24$ km s^{-1} in dense media (e.g. Hollenback & McKee 1980). The problem has been discussed widely in connection with YSO outflows and was highlighted in the case of CRL 618 by Burton & Geballe (1986) who advanced four possibilities for the very broad S(1) line profile in that object: (i) upscattering of H$_2$ photons off fast-moving dust grains; (ii) MHD shocks; (iii) reformation of H$_2$ on dust grains behind a fast-moving shock; (iv) H$_2$ emission from fast-moving clumps or bullets.

We discount the first possibility as in order to observe the clearly defined red- and blue-shifted outflows then the dust would have to be moving away from the H$_2$-emitting region in the NE lobe and toward it in the SW lobe, which seems contrived. In addition, the H$_2$ emission and scattered continuum peaks are spatially separated. MHD shocks are likely in an object with a highly-collimated jet, however, the critical velocity is only raised to $\simeq 50$km s^{-1} (e.g. Smith 1994) which is still far too low to explain the observations. Reformation of H$_2$ behind a fast, dissociative shock can occur on a timescale of $10^{16}/(n$ cm$^{-3})$ s (Smith, Khanzadyan & Davis 2003), or within a dynamical timescale of ~ 100 yr for IRAS 16342 if $n > 3 \times 10^6$ cm^{-3}. The reformed H$_2$ would then have to be heated to 1400 K in subsequent shocks in order to produce the observed line ratios.

Burton & Geballe (1986) favoured the fast-moving clump or "bullet" model for CRL 618, and this was also supported by Ueta, Fong & Meixner (2001) based on the clumpy nature of the NIR images. It is not clear yet whether fast moving clumps are responsible for the high-velocity H$_2$ emission in IRAS 16342 but the model has attractions. Firstly, a clumpy structure for the outflow is consistent with the high-velocity H$_2$O masers, which require local densities $\sim 10^9$ cm^{-3} (Elitzur 1992). The fact that the H$_2$ emission has similar kinematics to the masers (Sec. 3.4) implies that it too may arise in these clumps. Secondly, a clumpy outflow may offer an explanation for the asymmetric line profiles mentioned in Sec. 3.4.1, where a blue wing develops upstream of the H$_2$ peak in the blue-shifted lobe and a red wing in the red-shifted lobe: clumps of material, accelerated by the jet, will move ballistically, i.e. radially outward, in a direction determined by the jet orientation at that particular point in its precessional cycle when the interaction between the jet and the clump occurs. In Fig. 5 the contours of H$_2$ emission curve up (down) at the ends of the NE (SW) lobes, towards the H$_2$O maser positions, which lie off the nebula axis in a point-symmetric fashion. This presumably indicates the current projected orientation of the jet. Moving back along the nebula axis in the NE lobe, and hence back along the precessional spiral, we can speculate that the jet axis points predominantly behind the plane of the sky here, so that a red wing develops on the line (moving from a to c in Fig. 6) as the line of sight includes clumps with higher radial velocity. If the jet is point symmetric, then at an equivalent position in the SW lobe, its axis would be pointing towards the front surface of the lobe, producing a blue-shifted wing to the line, which would diminish towards the end of the blue lobe. However, the asymmetries in the line profiles appear quite pronounced, extending over several SINFONI spectral pixels in Fig. 6, whereas the shift in radial velocity corresponding to a precession angle of 10° amounts to only ~ 1 spectral channel for a jet speed of 155 km s^{-1}. An additional

source of asymmetry appears necessary and further observations with higher velocity- and spatial-resolution are needed to investigate these possibilities further.

4.4 Comparison with pre-MS outflows

Collimated outflows are thought to be an integral part of star formation, extracting angular momentum from a circumstellar disc and enabling accretion onto the protostar. In Class O YSOs (age $\leqslant 10^4$ yr) the outflows are mainly molecular, often with a fast $(10 - 100$ km s$^{-1})$ and highly collimated jet, traced in H$_2$, driving a slower $(\sim 10$ km s$^{-1})$ and wider-angle outflow of swept-up gas, traced by CO (see Cabrit, Ferreira & Dougados 2011 for a recent review). There are clearly similarities with post-AGB outflows such as IRAS 16342, CRL 618 and IRAS 22036+5306 (Sahai et al. 2006). The Class 0 outflow of HH 211 can be compared to IRAS 16342 including (i) a deeply-embedded driving source detected only at sub-millimetre wavelengths, (ii) outflow cavity structure traced in low-velocity CO emission with a high velocity axial component (Gueth & Guilloteau 1999) and (iii) shocked H$_2$ emission consistent with interaction of a jet with the ambient material (McCaughrean, Rayner & Zinnecker 1994). The HH211 jet itself is mapped in SiO $J = 8 - 7$ emission as a spectacular chain of knots extending > 15 arcsec on either side of the source into the H$_2$-emitting region (Lee et al. 2009b). Wiggles in the jet structure are interpreted as orbital motion of the jet source in a binary system, rather than precession (Lee et al. 2010)[3]. Further examples of well-studied YSO jets driving high-speed H$_2$ outflows include HH212 (Correia et al. 2009), and the Class 0/I outflows of HH34 and HH1 (Garcia Lopez et al. 2008).

4.4.1 Evidence for accretion discs

There is considerable evidence that protostellar jets are intimately linked with the presence of accretion discs, across a wide range of source masses and evolutionary stages from Class 0 to Class III. The correlation between outflow momentum and accretion rate (e.g. Richer et al. 2000 for Class 0 sources) has led to the concept of outflows as accretion-driven winds from magnetized circumstellar discs (see reviews by Königl et al. 2000 and Shu et al. 2000). It has been known for some time that the momentum and energy associated with many pre-PN outflows is too high to result from purely radiation-driven winds (Bujarrabal et al. 2001), and MHD models involving the launching of jets from accretion discs have been advanced in the evolved star case too (e.g. Soker & Rappaport 2000; Livio & Soker 2001; García-Arredondo & Frank 2004). In this case the formation of an accretion disc implies the presence of a binary companion (see De Marco 2009 for a review of binary interaction scenarios).

Using our extinction-corrected flux measurement of

$I_{1-0S(1)} = 2.97 \times 10^{-16}$ W m^{-2}, taking $d = 2$ kpc, and assuming that the $1-0$ S(1) line will contribute approximately 10 per cent of the total H$_2$ flux[4] gives $L_{H_2} = 0.37$ L$_\odot$. The H$_2$ luminosity of IRAS 16342 is therefore of the same order of magnitude as the majority of jet-active Class 0 and I protostellar sources studied by Caratti o Garatti et al. (2006). In the protostellar sources $L_{H_2}/L_{bol} \sim 0.04$ with the luminosity deriving from the accretion process, so that $L_{bol} \sim L_{acc}$. If the molecular outflow in IRAS 16342 is accretion powered then the accretion luminosity, $L_{acc} \sim 10$ L$_\odot$, is similar to that of a Class 0 protostellar source.

Bright CO bandhead emission and permitted atomic lines such as Na I, Ca I, Mg I have been observed around embedded protostellar sources associated with HH jets and are thought to be tracers of active accretion discs (e.g. Antoniucci et al. 2008). In a VLT-SINFONI study of seven HH jet systems associated with Class I sources, Davis et al. (2011) find that six sources (HH 34-IRS, HH300-IRS, SVS13, HH 72-IRS, HH999-IRS, HH 26-IRS) show strong CO bandhead emission as well as the atomic emission lines. In most cases the CO emission is coincident with the jet source locations, strengthening the association with the central accretion process, whereas the H$_2$ emission lines are offset from the source and therefore appear to trace the collimated outflows. In IRAS 16342, the CO bandheads and Na I line are seen in the scattered continuum so that their origin lies close to the illuminating source and therefore the jet source region. This provides further evidence that the jet in IRAS 16342 may be associated with an active accretion disc, with the CO bandhead emission arising either in the disc or in an accretion flow (Martin 1997). As the mass-losing star in IRAS 16342 evolves to higher temperatures and lower mass-loss rates, we may expect this molecular signature of accretion to diminish. It is interesting to note that there is little sign of CO bandhead emission in the spectrum of CRL 618 (Thronson 1981), which has a much hotter B0 central star, a HII region, and seems to be at a more advanced pre-PN phase.

5 CONCLUSIONS

Using integral field spectroscopy we have detected and imaged a fast, bipolar H$_2$ outflow from IRAS 16342-3814 (the Water Fountain) with the following properties:

(i) We detect the $v = 1 - 0$ S(0) to S(3), Q(1) to Q(4) and $v = 2 - 1$ S(1) and S(3) lines of H$_2$ in the K-band. Line diagnostics indicate shock-excitation with a gas temperature of 1400 K assuming LTE. There is some evidence for a higher temperature component of gas.

(ii) The H$_2$ emission peaks are located on the bipolar axis of the system at PA 68° but offset further from the source than the continuum peaks. The emission in the NE lobe is red-shifted relative to systemic and that in the SW lobe blue shifted.

(iii) Accounting for an inclination of the bipolar axis to the plane of the sky of 45°, the deprojected axial velocity of the H$_2$-emitting gas (away from the source) is 153 and 184 ± 24 km s^{-1} in the NE and SW lobes, respectively.

---

[3] Note that this interpretation is not applicable to the corkscrew structure of the IRAS 16342 jet: the diameter of the corkscrew is ≈ 0.25 arcsec or 500 au at 2 kpc, which is incompatible with an orbital period of ~ 50 yr in a stellar binary system

[4] see fig. 3 of Caratti o Garatti et al. (2006)

(iv) We see asymmetric line profiles, with the red-shifted H_2 emission in the NE lobe having a red wing and the blue-shifted emission in the SW lobe a blue wing. These wings become more pronounced with decreasing distance from the source, which we find difficult to account for in terms of a terminal bow shock model. Instead we suggest that the shocks may arise in fast-moving clumps, accelerated by the precessing jet. A clump interpretation may also provide a mechanism by which the H_2 can be excited in a low-velocity shock without dissociating, but exhibit the observed high-velocity bulk motion.

(v) From the $1 - 0\ S(1)$ line we estimate that the mass of shocked H_2 is $M_{H_2} = 1.9 \pm 0.5 \times 10^{-4}$ $M_\odot$ giving an outflow rate of $\dot{M}_{H_2} = 1.7 \pm 0.7 \times 10^{-6}$ $M_\odot$ yr^{-1}, comparable with the mass flux estimated from CO observations.

(vi) The luminosity in H_2, $L_{H_2} = 0.37$ $L_\odot$, is similar to that of Class 0 protostellar outflows which are thought to be powered by accretion discs. Evidence that the jet and outflow in IRAS 16342 are associated with accretion is provided by the detection of CO bandheads and a Na I feature in emission. These features are also observed in jet-active protostellar sources and are thought to trace hot gas in the inner regions of an accretion disc or flow.

The similarities between the bipolar H_2 outflow of IRAS 16342-3814 and those of protostellar sources support the possibility that molecular outflows at both ends of the main sequence may be powered by accretion-driven jets. In this way evolved stars nearing the ends of their lives may once again relive the energetic days of their youth.

ACKNOWLEDGMENTS

REFERENCES

Antoniucci S., Nisini B., Giannini T. & Lorenzetti L., 2008, A&A, 479, 503

Bonnet H., et al., 2004, The ESO Messenger, 117, 17

Bragg S.L., Brault J.W., Smith W.H., 1982, ApJ, 263, 999

Bujarrabal V., Castro-Carrizo A., Alcolea J., Sánchez Contreras C., 2001, A&A, 377, 868

Burton M.G., Geballe T.R., 1986, MNRAS, 223, 13p

Cabrit S., Ferreira J., Dougados C., 2011, Jets at all Scales, eds: Romero G.E., Sunyaev R.A. & Belloni T., IAU Symp. 275, p374

Caratti o Garatti A., Giannini T., Nisini B., Lorenzetti D., 2006, A&A, 449, 1077

Claussen M.J., Sahai R., Morris M.R., 2009, ApJ, 691, 219

Cliffe J.A., Frank A., Jones T.W., 1996, MNRAS, 282, 1114

Correia S., Zinnecker H., Ridgway S.T., McCaughrean M.J., 2009, A&A, 505, 673

Cox P., Huggins P.J., Maillard J.-P., Muthu C., Bachiller R., & Forveille T., 2003, ApJ, 586, L87

Davis C.J., Ray T.P., Desroches L., Aspin C., 2001, MNRAS 326, 524

Davis C.J., Smith M.D., Stern L., Kerr T.H., Chiar J.E., 2003, MNRAS 344, 262

Davis C.J., Cervantes B., Nisini B., Giannini T., Takami M., Whelan E., Smith M.D., Ray, T.P., et al., 2011, A&A, 528, A3

De Marco O., 2009, PASP, 121, 316

Eisenhauer F., et al., 2003, SPIE, 4841, 1548

Elitzur M., 1992, Astronomical Masers, Springer

García-Hernández D.A., Manchado A., García-Lario P., Domínguez-Tagle C., Conway G.M., Prada F., 2002, A&A, 387, 955

Garcia Lopez R., Nisini B., Giannini T., Eislöffel J., Bacciotti F., Podio L., 2008, A&A, 487, 1019

García-Arredondo F., Frank A., 2004, ApJ, 600, 992

García-Segura G., López J., Franco J., 2005, ApJ, 618, 919

Gledhill T.M., Forde K.P., Lowe K.T.E., Smith M.D., 2011, MNRAS, 411, 1453

Gledhill T.M., 2005, MNRAS, 356, 883

Gueth F., Guilloteau S., 1999, A&A, 343, 571

Gustafsson M., Ravkilde T., Kristensen L.E., Cabrit S., Field D., Pineau des Forêts G., 2010, A&A, 513, A5

He J.-H., Imai H., Hasegawa T.I., Campbell S.W., Nakashima J., 2008, A&A, 488, L21

Hollenbach D.J., McKee C.F., 1980, ApJ, 342, 306

Imai H., He J.-H., Nakashima J., Ukita N., Deguchi S., Koning N., 2009, PASJ, 61, 1365

Kastner J.H., Weintraub D.A., Gatley I., Henn L., 2001, ApJ, 546, 279

Königl A., Purdritz R.E., 2000, Protostars and Planets IV, eds: Mannings V., Boss A.P., Russell S. S., University of Arizona Press, p759

Lagadec E., et al., 2011, MNRAS, 417, 32

Lee C.-F., Sahai R., 2003, ApJ, 586, 319

Lee C.-F., Hsu M.-C., Sahai R., 2009, ApJ, 696, 1630

Lee C.-F., Hirano N., Palau A., Ho P.T.P., Bourke T.L., Zhang Q., Shang H., 2009b, ApJ, 699, 1584

Lee C.-F., Hasegawa T.I., Hirano N., Palau A., Shang H., Ho P.T.P., Zhang Q., 2010, ApJ, 713, 731

Likkel L., Morris M, 1988, ApJ, 329, 914

Likkel L., Morris M., Maddalena R.J., 1992, A&A, 256, 581

Livio M., Soker N., 2001, ApJ, 552, 685

Martin S.C., 1997, ApJ, 478, L33

McCaughrean M.J., Rayner J.T., Zinnecker H., 1994, ApJ, 436, L189

Murakawa K., Sahai, R., 2011, Asymmetrical Planetary Nebulae 5; eds: Zijlstra A.A., Lykou F., Lagadec E., McDonald I., A11.

Nakashima J.-I., Fong D, Hasegawa T., Hirano N., Koning N., Kwok S., Lim J., Trung D.-V., Young K., 2007, AJ, 134, 2035

Richer J.S., Shepherd D.S., Cabrit S., Bachiller R., Churchwell E., Protostars and Planets IV, eds: Mannings V., Boss A.P., Russell S. S., University of Arizona Press, 867

Rosen A., Smith M.D., 2004, MNRAS, 347, 1097

Sahai R., Trauger J.T., 1998, A.J., 116, 1357

Sahai R., te Lintel Hekkert P., Morris M.R., Zijlstra A., Likkel L., 1999, ApJ, 514, L115

Sahai R., le Mignant D., Sánchez Contreras C., Campbell R.D., Chaffee F.H., 2005, ApJ, 622, L53

Sahai R., Young K., Patel N.A., Sánchez Contreras C., Morris M., 2006, ApJ, 653, 1241

Sahai R., Morris M., Sánchez Contreras C., Claussen M.,

2007, A.J., 134, 2200

Sánchez Contreras C., Bujarrabal V., Castro-Carrizo A., Alcolea J., Sargent A., 2004, ApJ, 617, 1142

Schmidt G.D., Cohen M., 1981, ApJ, 246, 444

Schödel R., Najarro F., Muzic K., Eckart A., 2010, A&A, 511, 13

Schultz A.S.B., Burton M.G., Brand P.W.J.L., 2005, MN-RAS, 358, 1195

Shu F.H., Najita J.R., Shang H., Li Z.-Y., 2000, Protostars and Planets IV, eds: Mannings V., Boss A.P., Russell S. S., University of Arizona Press, p789

Shull J.M., Hollenbach D.J., 1978, ApJ, 220, 525

Siódmiak N., Meixner M., Ueta T., Sugerman B.E.K., Van de Steene G.C., Szczerba R., 2008, ApJ, 677, 382

Smith M.D., 1994, MNRAS, 266, 238

Smith M.D., Suttner G., Yorke H.W., 1997, A&A, 323, 223

Smith M.D., Khanzadyan T., Davis C.J., 2003, MNRAS, 339, 524

Smith M.D., Rosen A., 2005, MNRAS, 357, 579

Soker N., Rappaport S., 2000, ApJ, 538, 241

Stead J.J., Hoare M.G., 2009, MNRAS, 400, 731

Suttner G., Smith M.D., Yorke H.W., Zinnecker H., 1997, A&A, 318, 595

Szymczak M., Gérard E., 2004, A&A, 423, 209

te Lintel Hekkert P.,Habing H.J., Caswell J.L., Haynes R.F., Norris R.P., 1988, A&A, 202, L19

Thronson H.A., 1981, ApJ, 248, 984

Ueta T., Fong D., Meixner M., 2001, ApJ, 557, L117

Verhoelst T., Waters L.B.F.M., Verhoeff A., Van Winckel H., Pel J.W., Peletier R.F., 2009, A&A, 503, 837

Westbrook W.E., Becklin E.E., Merrill K.M., Neugebauer G., Schmidt M., Willner S.P., Wynn-Williams C.G., 1975, ApJ, 202, 407

Zijlstra A.A, Matsuura M., Dijkstra C., 2004, Asymmetrical Planetary Nebulae III, eds. Meixner M., Kastner J., Balick B., Soker N, ASP Conference Series, Vol. 313, 65

Zijlstra A.A, Chapman J.M., te Lintel Hekkert P., Likkel L., Comeron F., Norris R.P., Molster F.J., Cohen R.J., 2001, MNRAS, 322, 280